Implications of Refined Altimetry on the Estimates of Mesoscale Activity and Eddy-Driven Offshore Transport in the Eastern Boundary Upwelling Systems

Arthur Capet,[1] Evan Mason,[1] Vincent Rossi,[2] Charles Troupin,[3] Yannice Faugère,[4] Isabelle Pujol,[4] and Ananda Pascual[1]

[1]IMEDEA(CSIC-UIB), Esporles, Illes Balears, Spain

[2]IFISC, Palma de Mallorca, Illes Balears, Spain

[3]SOCIB, Palma de Mallorca, Illes Balears, Spain

[4]Space Oceanography Division, CLS, Toulouse, France.

This article has been accepted for publication and undergone full peer review but has not been through the copyediting, typesetting, pagination and proofreading process, which may lead to differences between this version and the Version of Record. Please cite this article as doi: 10.1002/2014GL061770

We investigate the extent to which the recently upgraded version of the Ssalto/Duacs sea level anomaly product affects the description of mesoscale activity in the Eastern Boundary Upwelling Systems (EBUS). Drifter observations confirm that the new data set released by AVISO in April 2014 (DT14) offers an enhanced description of mesoscale activity for the four EBUS. DT14 returns significantly higher eddy kinetic energy levels (+40-100%) within a 300 km coastal band, where mesoscale structures are known to induce important lateral physical and biogeochemical fluxes. When applied to DT14, an automatic eddy detection algorithm detects more eddies in the EBUS (+37%), and lower eddy radius estimates, in comparison with results using the former altimetry product (DT10). We show that, despite higher eddy densities, the smaller eddy radii result in westward eddy transport estimates that are smaller than those obtained from DT10 (-12%).

1. Introduction

Oceanic mesoscale circulation features, scaling from tens to hundreds of kilometers, play an essential role in the transport of water masses and therefore in the setting and maintenance of the global oceanic thermohaline structure [*McWilliams*, 1985; *Danabasoglu et al.*, 1994; *Zhang et al.*, 2013; *Dong et al.*, 2014]. Mesoscale structures also have considerable large scale impacts on oceanic productivity by inducing local vertical nutrient fluxes [*Oschlies and Garçon*, 1998; *Gaube et al.*, 2013], enhancing isopycnal diffusion [*Lee and Williams*, 2000], and generating advective transport across general circulation streamlines [*Williams and Follows*, 1998; *Sangrà et al.*, 2009].

Mesoscale activity can be assessed at the global scale from remotely-sensed observations of sea level anomalies (SLA). Gridded products, obtained after filtering and interpolation of "along-track" satellite measurements, are commonly used to assess the spatial and temporal variability of horizontal mesoscale activity [*Stammer*, 1997; *Ducet et al.*, 2000; *Pascual et al.*, 2006]. Converting raw satellite sensor signals to accessible and exploitable gridded products involves a number of processing steps, each of which is a compromise between the filtering out observational noise and the retention of the most relevant part of the original signal [*Le Traon and Dibarboure*, 1999; *Ducet et al.*, 2000]

After 20 years of observations the AVISO center went through a complete reprocessing of the Ssalto/Duacs sea level anomaly dataset in order to exploit the most recent advances in each of the successive processing steps and to provide a product of homogeneous quality. While the advantages of this reprocessing have been described at global

scale [*DUACS/Aviso*, 2014], this study focuses on its implications in the Eastern Boundary Upwelling Systems (EBUS).

Characterized by high primary production fueled by the upwelling of nutrient rich waters, EBUS account for around 20% of the global catch of marine fish despite covering less than 1% of the global ocean [*Pauly and Christensen*, 1995; *Chavez and Messié*, 2009]. The mechanisms ruling their biogeochemical variability are therefore of high societal concern.

Eddy kinetic energy (EKE), a measure of mesoscale activity, has moderate values in the EBUS (e.g., in comparison with western boundary currents) but its variability is known as one of the main drivers of primary production in these areas [*Rossi et al.*, 2009; *Lachkar and Gruber*, 2012].

The contribution of mesoscale activity to buoyancy [*Capet et al.*, 2008] and biogeochemical [*Gruber et al.*, 2011] fluxes in the EBUS is maximal within a narrow 300 km strip adjacent to the shore. This contribution mainly consists of an intensification of zonal transport by coherent mesoscale eddies and filaments, as well as an enhancement of isopycnal subduction processes [*Rossi et al.*, 2008, 2009; *Gruber et al.*, 2011; *Hernández-Carrasco et al.*, 2014].

The limited accuracy of altimetry products in nearshore areas [e.g. *Fu and Ubelmann*, 2014; *Bouffard et al.*, 2014] may have impeded a proper assessment of mesoscale dynamics in the EBUS. We therefore aim to show how the reprocessed AVISO altimetry product enhances the description of mesoscale activity in the EBUS regions.

2. The new SSALTO/Duacs AVISO altimetry product

In this study we use two altimeter products: the "DT14" (delayed-time 2014) and "DT10" that refer to the upgraded and former altimetry product, respectively. Both correspond to the delayed-time reference products ("two-sat" and "ref" in the revised and former AVISO nomenclature, respectively) that offer homogenous data quality over the entire data period through the use of just two satellites. In contrast, the "all-sat" or "upd" datasets from AVISO exploit all available satellites and therefore have higher but time-varying quality levels.

Employing several format modifications to better match user needs and international standards, the DT14 reprocessing also includes important modifications to the processing chain adopted to convert raw altimeter sensor signals to along-track and, finally, gridded sea level topography (e.g., new sensor-specific instrumental and atmospheric corrections, revised inter-calibration, a new ocean tidal component, new reference field). We refer to *DUACS/Aviso* [2014] for a detailed description of this revision and limit ourselves to a succinct description of the most relevant aspects. DT14 is computed directly on a 1/4° x 1/4° Cartesian grid, while DT10 is computed on a 1/3° x 1/3° Mercator grid. This results in a finer meridional resolution for the new product between the latitudes ±41.5°N. Beyond these latitudes only the zonal resolution is improved. Another important change in the DT mapping procedure is the change of the correlation scales used. The new scales better reproduce the spatial variability of the signal. The along-track filtering/sub-sampling applied to the along-track signal before mapping is also reduced (up to 30% at mid-latitudes) in order to be consistent with the new correlation scales.

To proceed with the comparison, DT10 SLA are interpolated onto the shifted DT14 grid and added to the reference field correction provided from the AVISO website (http://www.aviso.altimetry.fr/). Daily DT14 products are sub-sampled to match the weekly products available in DT10. Geostrophic currents and associated eddy kinetic energy (EKE) are computed from the SLA fields using a 5-point stencil method [*Arbic et al.*, 2012] for both datasets. This processing allows us to underline the changes and impacts of the SLA field only, as the respective DT10 and DT14 geostrophic velocity fields provided by AVISO are based on different MDTs and computational methods.

3. Sea Level Anomalies and Eddy Kinetic Energy

Figure 1a shows the standard deviation of the difference (σ_{14-10}) between the 20-year DT14 and DT10 SLA time series at each grid point, normalized by the local standard deviation estimated from DT14 (σ_{14}).

Global patterns of the normalized standard deviation of the difference present high values around southern subtropical latitudes and over most coastal/shelf areas. The southern hemisphere EBUS are particularly affected, but averaging $\sigma_{14-10}/\sigma_{14}$ in 50 km cross-shore distance bins reveals that the coastal increase is also visible for the northern hemisphere upwelling systems (Fig.1b-e).

The standard deviation of the difference is systematically associated with higher SLA variance in the DT14 products (not shown), which is concomitant with an increase in the EKE.

The global pattern of EKE relative increase (Fig. 2a) indicates high values along the coast and in the four EBUS regions. As western boundary currents have the highest

absolute EKE values (not shown), the relative increase is small, also probably due to the fact that larger eddies dominate in these regions [*Chelton et al.*, 2011].

EKE increase in the four EBUS is particularly high within 300 km from the coast with up to 100% relative increase in the Atlantic (Fig. 2b-e). We note that this increase is higher when EKE is derived using the 5-point stencil than when using the 3-point stencil (not shown). The high increases near the coast are therefore not due to the forced reduction of the stencil close to the coast.

4. Comparison with Surface Drifter Data

In this section, we investigate whether the higher mesoscale signals contained in DT14 effectively constitute an improved and realistic description of mesoscale activity in the EBUS. To assess this improvement we compare the geostrophic speeds (i.e., the magnitude of the velocities) derived from absolute dynamic topography (adding the mean dynamic topography [*Rio et al.*, 2011]) with those interpreted from in-situ drifters, obtained by subtracting the Ekman component and introducing a wind drift correction for those drifters that lost their drogues [*Rio and Hernandez*, 2003; *Rio*, 2012]. In this section we use the daily resolution of DT14 and equivalent daily fields from DT10 obtained by linear interpolation in time. Matches between drifters and satellite speeds are quantified by the skill score proposed by *Taylor* [2001] :

$$S = \frac{4(1+R)}{2(\frac{\sigma_{sat}}{\sigma_{drift}} + \frac{\sigma_{drift}}{\sigma_{sat}})^2} \quad (1)$$

where R is the Pearson correlation coefficient and σ_{sat} and σ_{drift} the standard deviation of satellite and drifter speeds, respectively. While no simple metric can satisfactorily capture the different aspects of error in a single number, we choose S as it penalizes both

amplitude and pattern mismatches, represented respectively by the variance ratio and the correlation coefficient. S_{14} (resp. S_{10}) represents the skill scores computed on the basis of DT14 sea level anomalies (resp. DT10).

Both S_{14} and S_{10} decrease near-shore (Fig. 3) indicating either a lower quality of the altimetry products near the shore, or greater errors associated with the drifter measurements (increased swell influence and/or deficiency of the Ekman model). Nevertheless, the use of DT14 altimetry systematically increases the skill scores. This increase is slightly higher in the near-shore regions for the California and Canary systems. For the Humboldt and Benguela systems, the lower number of available drifter tracks precludes a clear conclusion for a coastal increase of the skill score. Similar results are obtained when considering the velocity components independently.

These results demonstrate that the higher mesoscale activity resolved near the coast in the DT14 datasets truly offers an enhanced description of circulation features in the coastal regions of the EBUS.

Despite this improvement, this description remains incomplete as DT14 is still affected by limited resolution. An appreciation of this remaining resolution gap is provided by assessing the systematic relative bias between the magnitudes of satellite and drifter-derived velocities: $PB = \overline{(v_{sat} - v_{drift})}/\overline{v_{drift}}$, where v_{drift} and v_{sat} are respectively drifter and corresponding satellite velocities, the over-line representing the average.

Regional relative biases indicate that the geostrophic velocities derived from altimetry are systematically smaller than those derived from drifters. The underestimation obtained with DT10 ranges from 42 to 52% in the shelf regions (0-150 km) and from 28

to 41% in the offshore areas (450-600 km) of each EBUS. The use of DT14 reduces the underestimation to 30-36% and 18-30% in the inner and outer parts respectively. Despite a significant enhancement, the above result underlines the remaining limitation of state-of-the-art altimetry products [*Escudier et al.*, 2013]. Bootstrap iterations confirm that the confidence intervals ($p < 0.01$) obtained for S_{14} and S_{10} (resp. PB_{14} and PB_{10}) never overlap (Fig. 3), indicating that the skill score increases (resp. the percentage bias decreases) are significant in all cases.

5. Implications for Eddy Tracking and Lateral Transport Estimates

Satellite altimetry enables the automatic identification of individual eddy tracks and a statistical description of their geometrical and propagation characteristics [*Chelton et al.*, 2011].

Eddies have raised great interest in the oceanographic community because these structures are able to transport isolated water bodies over long distances. Highly non-linear eddies therefore significantly contribute to oceanic fluxes by transporting anomalies of physical and biogeochemical properties along their tracks, which do not necessarily follow large scale circulation patterns [e.g., *Sangrà et al.*, 2009]. If the non-linearity parameter of an eddy exceeds one, i.e., the ratio between its maximum orbital velocity U and its translation velocity c, it can be considered that the water mass within the eddy inner core, defined by closed zero-contours of potential vorticity, is transported conservatively [*Flierl*, 1981; *McWilliams*, 1985; *Early et al.*, 2011].

Accordingly, recent studies have attempted to evaluate the total volume of water transported within eddy cores and/or the corresponding physical and biogeochemical fluxes [*Sangrà et al.*, 2009; *Chaigneau et al.*, 2011; *Zhang et al.*, 2014; *Dong et al.*, 2014].

The lateral transport Q induced by eddies out of a given domain can be estimated using the outputs of an eddy-tracking experiment by considering

$$Q = \frac{1}{T} \sum_{i=1}^{n} V_i, \tag{2}$$

with T the duration of the experiment, n the total number of eddy tracks starting within the domain and crossing the domain boundary over the duration of the experiment, and V_i an estimate of individual eddy-core volume.

Assuming axial symmetry [*Chelton et al.*, 2011], the eddy-core volume can be described by the vertical integral $V = \pi \int [R(z)]^2 \, dz$, where $R(z)$ is a function describing the radial distance of the eddy-core contour at depth z.

Several volume approximation methods are based on the assumption that the radial and vertical components can be separated, i.e., that $R(z) = r.H(z)$, where r is the eddy radius estimated from altimetry and $H(z)$ is a local estimate of the eddy vertical structure that is independent of the altimetry data. These comprise methods assimilating eddies to simple geometric shapes of fixed depth [e.g. *Sangrà et al.*, 2009; *Dencausse et al.*, 2010], but also more complex composite analyzes exploiting synchronously available subsurface observations (e.g., ARGO floats) [e.g. *Chaigneau et al.*, 2011; *Zhang et al.*, 2013].

Under these assumptions (cf. discussion in auxiliary material), we can simplify the ratio between total eddy transport estimates derived from DT14 and DT10 to:

$$\frac{Q_{14}}{Q_{10}} = \frac{\sum_{i=1}^{n_{14}} r_{14,i}^2}{\sum_{j=1}^{n_{10}} r_{10,j}^2}. \quad (3)$$

To evaluate the potential impact of the refined altimetry product on such transport estimates we compute eddy tracks and associated geometric characteristics within all the EBUS by applying a sea surface height (SSH) based eddy tracking algorithm [*Mason et al.*, 2014] for the period 1993-2013. The eddy tracking is applied to the DT14 and DT10 datasets in their original forms (no interpolation or reference field correction). For consistency, daily DT14 products were subsampled to match the weekly resolution of DT10.

We identified the greatest eddy densities (i.e., average annual number of individual eddy tracks lasting more than 28 days) between 150 and 300 km from the coast in three of the four EBUS (California, Humboldt, Canary, Fig.4). This transitional region between the productive coastal upwelling and the oligotrophic open ocean is precisely where previous studies have evidenced the major contribution of eddies to lateral transport in these three systems [*Capet et al.*, 2008; *Gruber et al.*, 2011]. The open eastern boundary at the south of the Benguela system makes it particular from the other systems and it is therefore not surprising to find greater eddy densities in the offshore parts, influenced by the Agulhas retroflection.

As expected from the previous sections, the eddy tracking procedure evidences more eddies when applied on DT14 SLA (at least 10% in offshore regions) and this relative increase is greater nearshore (up to 30-70%, Fig.4).

The finer resolution of the DT14 altimetry products also affects the statistical distribution of eddy characteristics. Sharper DT14 SLA gradients leads to a general shift in the distribution towards smaller eddy radii (referring to the speed-based radius [*Mason et al.*, 2014; *Chelton et al.*, 2011]) and higher orbital velocities (Fig. 5). It is important to note that DT14 not only depicts more small eddies (< 70km) but also less large eddies (> 70km). This is attributed to the fact that smoothed altimetry products can lead to an overestimation of the radius of large eddies. The distributions of other eddy characteristics such as amplitude, translation velocity and life time are nearly unchanged (more details and specific distributions for each EBUS are given in the auxiliary material).

To assess the sensitivity of the westward eddy transport to the resolution of altimetry (Eq. 3), we counted the number n of eddies traveling from the coastal areas across the 300 km offshore limit and recorded their specific radius (averaged along each eddy track). Only eddies with a ratio $U/c > 1$ were considered.

While n_{14} is larger than n_{10} in each domain (respectively by +8.5, +18.2, +11.1, and +11.8 % for California, Canary, Humboldt and Benguela systems) the reduction of eddy radii results in an overall decrease of the total transport estimates (with Q_{14}/Q_{10}= -13.8, -10.5, -16.1 and -9.6% for California, Canary, Humboldt and Benguela). This counterintuitive result is due to the fact that the eddy radius has a quadratic impact on the volume estimate. The reduction of large eddy radii therefore has a greater effect on the total transport estimate than the addition of smaller eddies.

Note that these reduced numbers are valid for any geometrical method and that, at this point, we have not specified any particular volume estimation method.

The variability of eddy subsurface structure across the different regions [*Petersen et al.*, 2013] clearly indicates that model studies or, at the least, composite analyzes are required for a proper assessment of eddy induced lateral export from the coastal domain of the EBUS. It is important to add that volume estimates from altimetry that take eddy nonlinearity into account could have further impacts on transport estimates, since DT14 also affects the distribution of eddy nonlinearity (shifted towards higher values). These approaches are beyond the scope of the present study. We do nonetheless provide an estimate for the eddy lateral export across the 300 km offshore range of each EBUS based on the simplest method. We assume that eddy cores have the shape of half ellipsoids with circular surface section and fixed vertical extent Z.

Considering the extrema $Z = 200\,m$ and $Z = 600\,m$ results in Q_{14} ranges of $[5.0 - 14.9]$, $[2.8 - 8.5]$,$[4.3 - 13.1]$, $[3.6 - 10.9]$ Sv for the California, Canary, Humboldt and Benguela systems, respectively.

California, characterized here by the highest eddy-induced offshore transport, is also known to have the lowest offshore Ekman transport and the highest mesoscale turbulence (as deduced from a Lagrangian diagnostic of horizontal mixing) among all EBUS [*Rossi et al.*, 2009]. *Marchesiello and Estrade* [2009] suggested that biogeochemical coastal properties would be eroded more significantly in systems with particularly high eddy activity (such as California) than in other systems in which Ekman currents would govern offshore transport. *Combes et al.* [2013] recently found that cross-shore transport of coastal waters off California is indeed linked to both linear (Ekman upwelling) and non-linear (mesoscale eddies) dynamics, with the former process driving the cross-shelf transport of upwelled

water masses (i.e. of subsurface origins) and the latter controlling the net horizontal cross-shelf surface transport and extending deeper than the Ekman layer. While the correspondence between the levels of mesoscale horizontal mixing (as measured by Eulerian -EKE- or Lagrangian -FSLEs- surface diagnostics) and the magnitude of the eddy-induced offshore transport is not direct in other EBUS, our improved descriptions of mesoscale activity in EBUS are necessary to determine unambiguously whether mesoscale eddies or mean Ekman flow dominate offshore transport of coastal biogeochemical properties in these productive systems.

To conclude this section, we note that the relative increases of eddy density (Fig. 4) are higher in the regions presenting high EKE increases (Fig. 2), e.g., in the Atlantic EBUS compared to the Pacific EBUS or in the Humboldt compared to the California system. This suggests that more eddies are also to be expected in the open ocean where DT14 depicts high EKE increases. Alternatively, eddy density may remain the same but smaller measured eddies would result in higher EKE since the SLA spectrum is peaked at higher wavenumbers.

6. Conclusions

The present study establishes that the new SSALTO/Duacs altimetry products enhance the description of mesoscale activity in coastal regions of EBUS, precisely where previous studies have evidenced an important contribution of mesoscale activity in setting the structure of physical and biogeochemical export toward the open ocean. Previous observation-based studies of the relationship between mesoscale activity and biological production in these regions [*Rossi et al.*, 2008, 2009; *Gruber et al.*, 2011; *Lachkar and*

Gruber, 2012; *Hernández-Carrasco et al.*, 2014] might therefore have been impeded by the restricted description of mesoscale activity in EBUS. The present study therefore appeals for a reassessment of these relationships exploiting the new SSALTO/Duacs altimetry products.

Applying eddy tracking algorithms to the refined altimetry data set results in higher eddy densities but also in a shifted distribution of their radii towards smaller values. We show that, for a large range of volume transport estimation methods, the AVISO DT14 revision results in an average 12.5% reduction of estimated eddy lateral transports out of of the four EBUS.

While we focus here on the EBUS, Fig. 2 indicates that the DT14 revision also significantly affects the description of mesoscale activity in other coastal and open areas of the world ocean, and it might be expected that this revision would similarly impact automatically detected eddy censuses and properties, as well as derived transport estimates. The preceding conclusions call for an assessment of the implications of the DT14 altimetry revision on the recently published global estimates of eddy-induced lateral transport, which are critically dependent on the eddy radial characteristics derived from the altimetry products. More fundamentally, one might want to investigate the general implication that correlation length scales used to produce gridded altimetry products may bear on final transport estimates. While the inability of current altimeters to detect small scale structures has already been pointed out and addressed [*Keating et al.*, 2012], the present study shows that the limited resolution in contemporary altimetry products may also re-

sult in an overestimation of the radii of large eddies, leading to a quadratic impact on transport estimates.

Clearly, the expected finer altimeter resolution granted by the SWOT project will greatly clarify these matters [*Durand et al.*, 2010; *Fu and Ubelmann*, 2014].

Acknowledgments. This study was funded by the EU MyOcean2 project (EU N° FP7-SPA.2011.1.5-01-Grant Agreement 283367). Altimeter products are produced by SSALTO/DUACS and distributed by AVISO. Drifter data were provided by AOML and processed by CLS. V.R. acknowledges support from MICINN and FEDER through the ESCOLA project (CTM2012-39025-C02-01). E.M. is supported by a Spanish government JAE Doc grant (CSIC), cofinanced by FSE.

References

Arbic, B. K., R. B. Scott, D. B. Chelton, J. G. Richman, and J. F. Shriver (2012), Effects of stencil width on surface ocean geostrophic velocity and vorticity estimation from gridded satellite altimeter data, *J Geophys Res-Oceans*, *117*(C3).

Bouffard, J., F. Nencioli, R. Escudier, A. M. Doglioli, A. A. Petrenko, A. Pascual, P.-M. Poulain, and D. Elhmaidi (2014), Lagrangian analysis of satellite-derived currents: Application to the North Western Mediterranean coastal dynamics, *Adv Space Res*, *53*(5), 788–801.

Capet, X., F. Colas, J. C. McWilliams, P. Penven, and P. Marchesiello (2008), *Eddies in Eastern Boundary Subtropical Upwelling Systems*, pp. 131–147, American Geophysical Union, doi:10.1029/177GM10.

Chaigneau, A., M. Le Texier, G. Eldin, C. Grados, and O. Pizarro (2011), Vertical structure of mesoscale eddies in the eastern South Pacific Ocean: A composite analysis from altimetry and Argo profiling floats, *J Geophys Res-Oceans*, *116*(C11).

Chavez, F. P., and M. Messié (2009), A comparison of eastern boundary upwelling ecosystems, *Progr Oceanogr*, *83*(1), 80–96.

Chelton, D. B., M. G. Schlax, and R. M. Samelson (2011), Global observations of nonlinear mesoscale eddies, *Progr Oceanogr*, *91*(2), 167–216.

Combes, V., F. Chenillat, E. Di Lorenzo, P. Rivière, M. Ohman, and S. Bograd (2013), Cross-shore transport variability in the California Current: Ekman upwelling vs. eddy dynamics, *Progr Oceanogr*, *109*, 78–89.

Danabasoglu, G., J. C. McWilliams, P. R. Gent, et al. (1994), The role of mesoscale tracer transports in the global ocean circulation, *Science-AAAS-Weekly Paper Edition-including Guide to Scientific Information*, *264*(5162), 1123–1125.

Dencausse, G., M. Arhan, and S. Speich (2010), Routes of Agulhas rings in the southeastern Cape Basin, *Deep-Sea Res Pt I*, *57*(11), 1406–1421.

Dong, C., J. C. McWilliams, Y. Liu, and D. Chen (2014), Global heat and salt transports by eddy movement, *Nature Commun*, *5*.

DUACS/Aviso team (2014), A new version of SSALTO/Duacs products available in April 2014. Version 1.1, CNES, http://www.aviso.altimetry.fr/fileadmin/documents/data/duacs/Duacs2014.pdf.

Ducet, N., P.-Y. Le Traon, and G. Reverdin (2000), Global high-resolution mapping of ocean circulation from TOPEX/Poseidon and ERS-1 and-2, *J Geophys Res-Oceans*,

105(C8), 19,477–19,498.

Durand, M., L.-L. Fu, D. P. Lettenmaier, D. E. Alsdorf, E. Rodriguez, and D. Esteban-Fernandez (2010), The surface water and ocean topography mission: Observing terrestrial surface water and oceanic submesoscale eddies, *Proc. IEEE*, *98*(5), 766–779.

Early, J. J., R. Samelson, and D. B. Chelton (2011), The evolution and propagation of quasigeostrophic ocean eddies, *J Phys Oceanogr*, *41*(8), 1535–1555.

Escudier, R., J. Bouffard, A. Pascual, P.-M. Poulain, and M.-I. Pujol (2013), Improvement of coastal and mesoscale observation from space: Application to the northwestern Mediterranean Sea, *Geophys Res Lett*, *40*(10), 2148–2153.

Flierl, G. R. (1981), Particle motions in large-amplitude wave fields, *Geophys Astro Fluid*, *18*(1-2), 39–74.

Fu, L.-L., and C. Ubelmann (2014), On the transition from profile altimeter to swath altimeter for observing global ocean surface topography, *J Atmos Ocean Tech*, *31*(2), 560–568.

Gaube, P., D. Chelton, P. Strutton, and M. J. Behrenfeld (2013), Satellite observations of chlorophyll, phytoplankton biomass, and Ekman pumping in nonlinear mesoscale eddies, *J Geophys Res-Oceans*, *118*(12), 6349–6370.

Gruber, N., Z. Lachkar, H. Frenzel, P. Marchesiello, M. Münnich, J. C. McWilliams, T. Nagai, and G.-K. Plattner (2011), Eddy-induced reduction of biological production in eastern boundary upwelling systems, *Nature Geosci*, *4*(11), 787–792.

Hernández-Carrasco, I., V. Rossi, E. Hernández-García, V. Garçon, and C. López (2014), The reduction of plankton biomass induced by mesoscale stirring: A modeling study in

the Benguela upwelling, *Deep-Sea Res Pt I*, *83*, 65–80.

Keating, S. R., A. J. Majda, and K. S. Smith (2012), New methods for estimating ocean eddy heat transport using satellite altimetry, *Mon Weather Rev*, *140*(5), 1703–1722.

Lachkar, Z., and N. Gruber (2012), A comparative study of biological production in eastern boundary upwelling systems using an artificial neural network, *Biogeosciences*, *9*, 293–308.

Le Traon, P. Y., and G. Dibarboure (1999), Mesoscale mapping capabilities of multiple-satellite altimeter missions, *J Atmos Ocean Tech*, *16*(9), 1208–1223.

Lee, M.-M., and R. G. Williams (2000), The role of eddies in the isopycnic transfer of nutrients and their impact on biological production, *J Mar Res*, *58*(6), 895–917.

Marchesiello, P., and P. Estrade (2009), Eddy activity and mixing in upwelling systems: a comparative study of Northwest Africa and California regions, *Int J Earth Sci*, *98*(2), 299–308.

Mason, E., A. Pascual, and J. C. McWilliams (2014), A new sea surface height–based code for oceanic mesoscale eddy tracking, *J Atmos Ocean Tech*, *31*(5), 1181–1188.

McWilliams, J. C. (1985), Submesoscale, coherent vortices in the ocean, *Rev Geophys*, *23*(2), 165–182, doi:10.1029/RG023i002p00165.

Oschlies, A., and V. Garçon (1998), Eddy-induced enhancement of primary production in a model of the North Atlantic Ocean, *Nature*, *394*(6690), 266–269.

Pascual, A., Y. Faugère, G. Larnicol, and P.-Y. Le Traon (2006), Improved description of the ocean mesoscale variability by combining four satellite altimeters, *Geophys Res Lett*, *33*(2).

Pauly, D., and V. Christensen (1995), Primary production required to sustain global fisheries, *Nature*, *374*(6519), 255–257.

Petersen, M. R., S. J. Williams, M. E. Maltrud, M. W. Hecht, and B. Hamann (2013), A three-dimensional eddy census of a high-resolution global ocean simulation, *J Geophys Res-Oceans*, *118*(4), 1759–1774.

Rio, M.-H. (2012), Use of altimeter and wind data to detect the anomalous loss of SVP-type drifter's drogue, *J Atmos Ocean Tech*, *29*(11), 1663–1674.

Rio, M.-H., and F. Hernandez (2003), High-frequency response of wind-driven currents measured by drifting buoys and altimetry over the world ocean, *J Geophys Res-Oceans*, *108*(C8).

Rio, M.-H., S. Guinehut, and G. Larnicol (2011), New CNES-CLS09 global mean dynamic topography computed from the combination of GRACE data, altimetry, and in situ measurements, *J Geophys Res-Oceans*, *116*(C7).

Rossi, V., C. López, J. Sudre, E. Hernández-García, and V. Garçon (2008), Comparative study of mixing and biological activity of the Benguela and Canary upwelling systems, *Geophys Res Lett*, *35*(11).

Rossi, V., C. López, E. Hernández-García, J. Sudre, V. Garçon, and Y. Morel (2009), Surface mixing and biological activity in the four Eastern Boundary Upwelling Systems, *Nonlinear Proc Geoph*, *16*, 557–568.

Sangrà, P., A. Pascual, Á. Rodríguez-Santana, F. Machín, E. Mason, J. C. McWilliams, J. L. Pelegrí, C. Dong, A. Rubio, J. Arístegui, et al. (2009), The Canary Eddy Corridor: A major pathway for long-lived eddies in the subtropical North Atlantic, *Deep-Sea Res*

Pt I, *56*(12), 2100–2114.

Stammer, D. (1997), Global characteristics of ocean variability estimated from regional TOPEX/POSEIDON altimeter measurements, *J Phys Oceanogr*, *27*(8), 1743–1769.

Taylor, K. E. (2001), Summarizing multiple aspects of model performance in a single diagram, *J. Geophys. Res.*, *106*(D7), 7183–7192, doi: http://dx.doi.org/10.1029/2000JD900719.

Williams, R. G., and M. J. Follows (1998), The Ekman transfer of nutrients and maintenance of new production over the North Atlantic, *Deep-Sea Res Pt I*, *45*(2), 461–489.

Zhang, Z., Y. Zhang, W. Wang, and R. X. Huang (2013), Universal structure of mesoscale eddies in the ocean, *Geophys Res Lett*, *40*(14), 3677–3681.

Zhang, Z., W. Wang, and B. Qiu (2014), Oceanic mass transport by mesoscale eddies, *Science*, *345*(6194), 322–324.

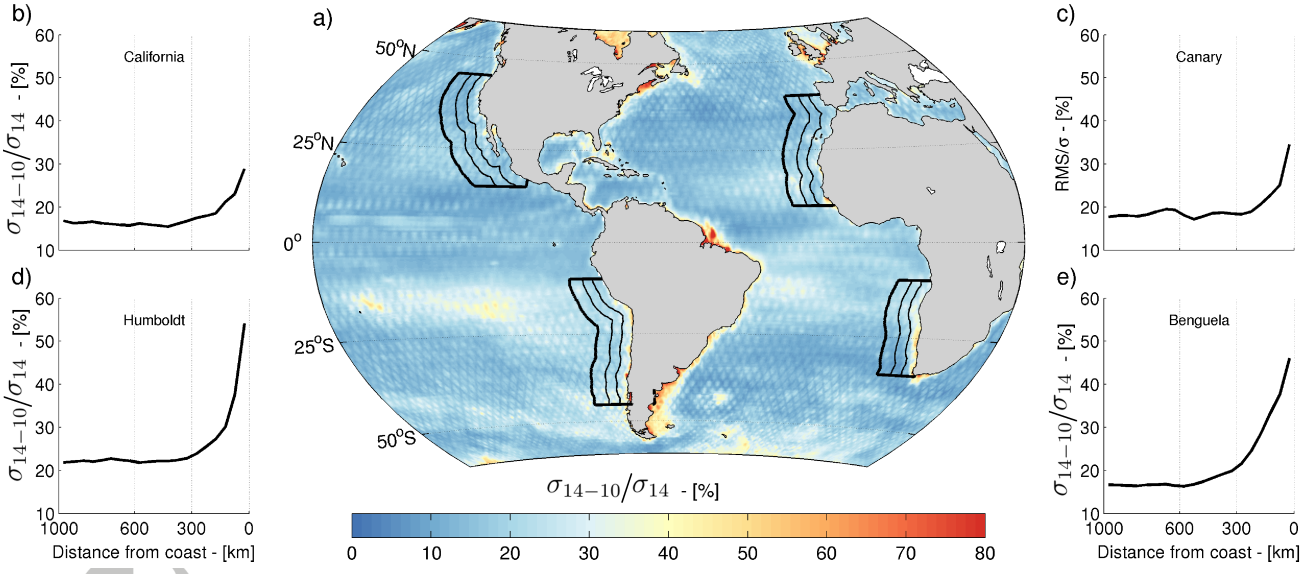

Figure 1. Standard deviation of the difference between DT10 and DT14 SLA normalized by the local DT14 SLA standard deviation. (a) Global spatial pattern. The black lines indicate (bold) the EBUS domains and (thin) the 300 and 600 km cross-shore distance ranges. (b-e) EBUS regional values averaged for successive cross-shore distances ranges.

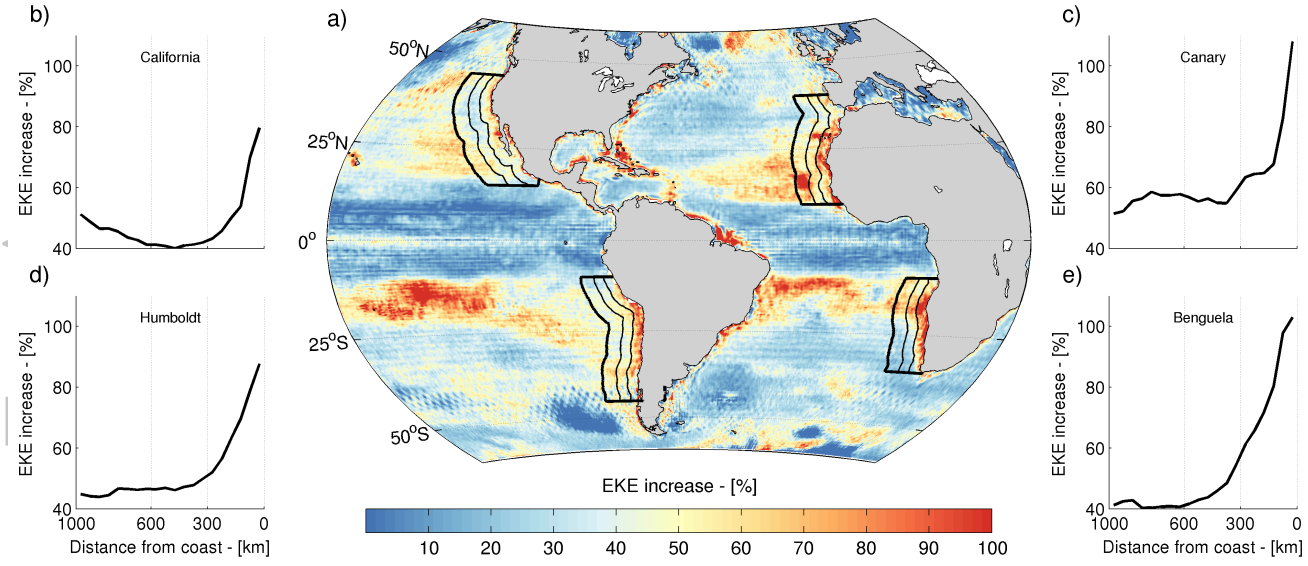

Figure 2. Relative increase of Eddy Kinetic Energy when derived from DT14 instead of DT10 sea level anomalies. (a) Global spatial pattern. (b-e) EBUS regional values averaged for successive cross-shore distances ranges.

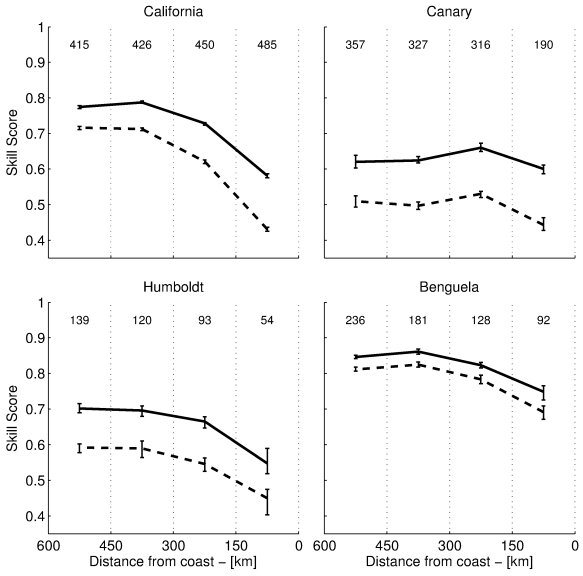

Figure 3. Skill scores quantifying the matches between satellite and drifter derived geostrophic velocities in different cross-shore distance ranges for (plain line) DT14 (dotted line) DT10 dataset. The number of available drifters for each distance range is indicated on the top of each panel.

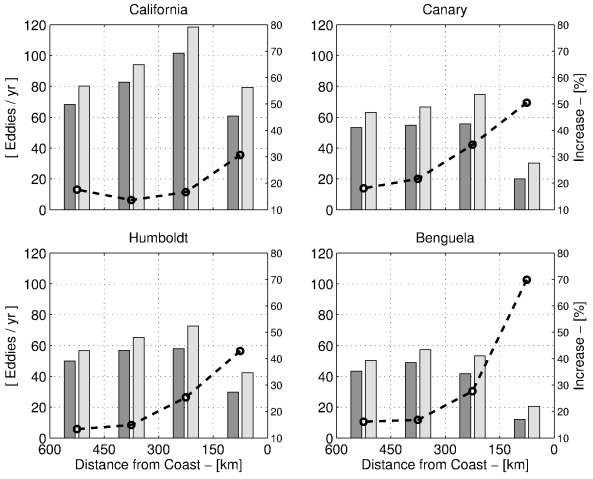

Figure 4. Eddy density (vertical scale on the left of each panel) in successive cross-shore distance ranges for the four EBUS, detected from (dark gray) DT10 and (light gray) DT14 datasets. The dashed lines indicate the relative increase between eddy density estimated from DT14 and DT10 (vertical scale on the right of each panel).

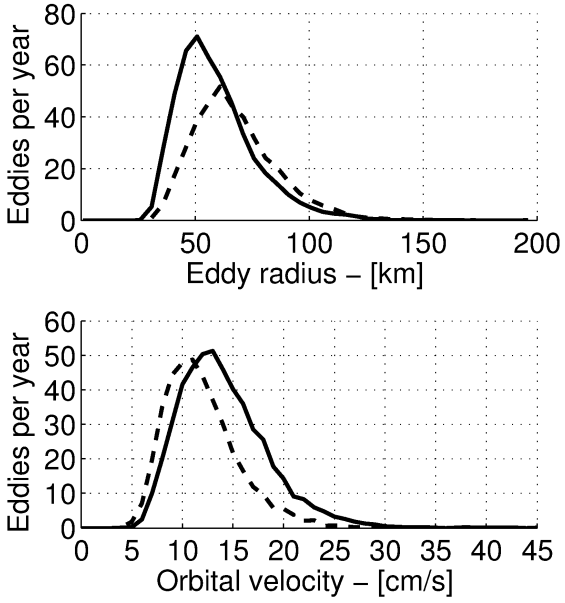

Figure 5. Distribution of (upper panel) eddy radii (5 km bins) and (lower panel) orbital velocity (1 cm/s bins) obtained from eddy tracking applied on (plain line) DT14 and (dotted line) DT10 altimetry products in the California system. The distribution considers all weekly occurrences of both cyclonic and anticyclonic eddies within 300 km from the coast. Amplitudes, translation speeds and eddy lifetimes depict nearly identical distribution (not shown).